International Journal of Mass Spectrometry 308 (2011) 281–288

Contents lists available at ScienceDirect

International Journal of Mass Spectrometry

journal homepage: www.elsevier.com/locate/ijms

N–H$^+$ vibrational anharmonicities directly revealed from DFT-based molecular dynamics simulations on the Ala_7H^+ protonated peptide

Amel Sediki [a], Lavina C. Snoek [b], Marie-Pierre Gaigeot [a,c,*]

[a] Université d'Evry val d'Essonne, LAMBE UMR8587 Laboratoire Analyse et Modélisation pour la Biologie et l'Environnement, Blvd F. Mitterrand, Bât. Maupertuis, 91025 Evry, France
[b] Physical and Theoretical Chemistry Laboratory, Chemistry Department, University of Oxford, South Parks Road, Oxford OX1 3QZ, United Kingdom
[c] Institut Universitaire de France (IUF), 103 Blvd St Michel, 75005 Paris, France

ARTICLE INFO

Article history:
Received 22 May 2011
Received in revised form 19 June 2011
Accepted 23 June 2011
Available online 30 June 2011

Keywords:
DFT-based molecular dynamics
Infrared spectroscopy
Peptide
Gas phase
IRMPD
Vibrational anharmonicity

ABSTRACT

The present investigation reports DFT-based Born–Oppenheimer molecular dynamics simulations of the gas phase Ala_7H^+ protonated peptide, in order to unravel the structure and dynamics of the peptide and its Infrared vibrational signatures. At 350 K, the most statistically relevant conformations adopted by the globular folded Ala_7H^+ peptide have the NH_3^+ N-terminus involved in two $NH^+ \rightarrow O{=}C$ charge-solvated hydrogen bonds. The dynamics performed here nicely provide a clear understanding of the IR-MPD features experimentally recorded, with an excellent matching of the dynamically simulated IR spectrum with the experiment in terms of band-positions and band-shapes. In particular, the diverse vibrational anharmonicities displayed by the N–H$^+$ stretches depending on the number of simultaneous hydrogen bonds that the NH_3^+ can form at the N-terminus of the Ala_7H^+ peptide chain, are remarkably reproduced by the present dynamics at finite temperature. This gives rise to a proper understanding of the different IR active bands, especially the supplementary band between 3100 and 3300 cm^{-1} present for the Ala_7H^+ peptide and absent for the smaller peptide chain lengths. Vibrational anharmonicities are naturally taken into account in the dynamical treatment of the movements, and this has once more been illustrated in the present work. Our results on the N–H$^+$ stretching motions in relation with the number of hydrogen bonds formed by the NH_3^+ group, can be used as general guidelines in order to precisely interpret IR-MPD spectra of molecules containing NH_3^+ groups, taking into account vibrational anharmonicities.

1. Introduction

The past decade has witnessed the development of several experimental set-ups in order to probe the vibrational properties of polypeptides in the gas phase [1–3], unravelling their three-dimensional organisation, and directly probing their intrinsic properties without interactions arising from the surrounding solvent environment. These experiments can mainly be separated into two groups, with low temperature gas phase infrared spectroscopy on the one hand [4–7,1], and room temperature gas phase spectroscopy based on "action spectroscopy" on the other hand. Action spectroscopy makes use either of a messenger method (IR-PD, Infrared Photon Dissociation) [8–11] or of Multi-Photon Dissociation (IR-MPD, Infrared Multi Photon Dissociation) [12–17]. Simons et al. [18,16,19] have also developed a photochemical method for producing protonated biological molecules in a supersonic expansion, thus avoiding the initial mass spectrometry selection inherent to the other IR-MPD techniques. These experiments have been successfully applied to structural analyses of biomimetic molecules and peptides [15,20,14,21–24,16,19,25] and more elaborate biomolecules [26,27,1,28]. Studies of unsolvated peptides and proteins are not just of fundamental interests: while the interactions with the solvent are obviously important, as water is an ubiquitous environment of biomolecules, the solvent is nonetheless excluded in many environments such as in the hydrophobic interior of folded proteins or is highly shielded as in membranes. As a consequence, the fundamental understanding of IR signatures of gas-phase secondary structures can thus be used in order to interpret the more complicated IR signatures of proteins in their natural environments. Gas-phase spectroscopy in conjunction with theoretical calculations offers the opportunity to dissect and analyse the counterbalancing forces that control the structures and their IR fingerprints.

Theoretical calculations have become essential in order to get a precise understanding of the experimental vibrational features and untangle the complexity and the congestion of the bands in relation with the underlying 3D structures and their dynamical

* Corresponding author at: Université d'Evry val d'Essonne, LAMBE UMR8587 Laboratoire Analyse et Modélisation pour la Biologie et l'Environnement, Blvd F. Mitterrand, Bât. Maupertuis, 91025 Evry, France.
E-mail address: mgaigeot@univ-evry.fr (M.-P. Gaigeot).
URL: http://www.lambe.univ-evry.fr/mpgaigeot/ (M.-P. Gaigeot).

1387-3806/$ – see front matter © 2011 Elsevier B.V. All rights reserved.
doi:10.1016/j.ijms.2011.06.016

properties. The finite temperature present in the gas phase IR-MPD experiments makes it necessary to apply theoretical tools which indeed take temperature into account, in order to accurately interpret the vibrational signatures, as we have recently reviewed [29]. Taking into account the dynamics of the molecules and its consequences on the measured properties such as vibrational spectra, can be achieved through molecular dynamics (MD) simulations. The calculation of infrared spectra through MD relies on dipole time correlation functions recorded along the trajectory [30,29]. Within the past few years, our group has shown that DFT-based molecular dynamics is a proper method for the calculation of IR spectra of peptide building blocks, in the gas phase or immersed in liquid water [31–33,25,34–36], at finite temperature. See our review on the subject [29]. One advantage of MD simulations for the calculation of IR spectra is that vibrational anharmonicities are taken into account in the final spectrum, in a direct way [29,37].

This particular point is the object of the present investigation, where we focus on the vibrational spectroscopy of the Ala_7H^+ protonated peptide in the gas phase. Our interest in that peptide follows up on our previous theoretical investigations on the spectroscopy of the Ala_2H^+ [33,25] and Ala_3H^+ [34] protonated ions. The IR-MPD experiments performed by Vaden et al. [19] on the series of Ala_n H^+ peptides has indeed shown that a supplementary vibrational band is observed in the IR-MPD spectrum of Ala_7H^+, clearly absent from the spectra of the smaller peptide chain-lengths (and maintained in longer peptide chains). Geometry optimisations and harmonic spectra calculations performed in Ref. [19] have shown that a new type of conformations is adopted by Ala_7H^+: folded globular structures which can only be obtained once a long enough peptidic chain is encountered. With these structural features and their related harmonic signatures, Vaden et al. [19] showed that structures where the NH_3^+ N-terminus of the protonated peptide is fully charge-solvated (in other words, the NH_3^+ is involved in three Hbonds with surrounding C=O sites) display vibrational signatures arising from the NH_3^+ group that could be compatible with the supplementary band seen around 3175 cm^{-1}. Conformations where the NH_3^+ is not fully charge-solvated, i.e., involved in two or one Hbond, could nonetheless not be fully ruled out, as they also displayed vibrational signatures compatible with that domain (although maybe to a lesser extent) and with higher frequency parts of the experimental spectrum. $NH^+\cdots O$ Hbonds are however intrinsically vibrationnally anharmonic, and it might seem surprising that a theoretical harmonic treatment is enough to provide a comprehensive view of such complex vibrations. Furthermore, the experimental spectrum displays peaks within the 2500–2900 cm^{-1} region that can not be accounted for by the harmonic spectra. In this region, highly anharmonic movements should be responsible for signatures, and one goal of the present work is also to dissect these.

We thus employ here DFT-based molecular dynamics simulations on the gas phase Ala_7H^+ protonated peptide in order to shed some light on these particular points related to vibrational anharmonicities. The finite temperature dynamics performed here at about 350 K not surprisingly also reveal highly interesting dynamical behaviours of the $NH^+\cdots O$ Hbonds between the NH_3^+ N-terminus and its surrounding. In particular, we show that folded structures with two $NH^+\cdots O$ Hbonds are statistically the most probable to occur at 350 K. The spectral features of these two $NH^+\cdots O$ Hbonded conformations provide a vibrational band which is in excellent agreement with the supplementary band observed in the experimental spectrum. We also show that a fully charge-solvated NH_3^+ group provides far less NH^+ vibrational anharmonicities, while conformations with one $NH^+\cdots O$ Hbond on average display highly red-shifted anharmonic stretches which are then identical to the vibrations obtained in the smaller Ala_3H^+ protonated peptide [34]. The supplementary IR-MPD experimental band observed in Ala_7H^+ is thus due to two $NH_3^+\cdots O$ Hbonded conformations, and this band directly reflects the extend of the H-bond network formed by NH_3^+ in the protonated alanine peptide Ala_nH^+ series.

Our paper summarizes the IR-MPD experiments from Vaden et al. [19] that are used as a support for the present theoretical investigation, and the DFT-based molecular dynamics simulations performed in the present work. We then present results on the dynamical behaviour of Ala_7H^+ at room temperature and the anharmonic vibrations of the NH_3^+ N-terminus of Ala_7H^+. Conclusions and perspectives end this paper.

2. Methods

The experimental IR-MPD method has been thoroughly described in previous papers, for more details see Refs. [19,34], and only a brief description is given here. The experimental results described herein are taken from Ref. [19]. Ala_7H^+ ions were generated by a photochemical protonation scheme, described in detail elsewhere [38,39,16]. As discussed in previous works, the 'temperature' of the Ala_7H^+ ions are not well-characterized but could be anywhere from 250 K to more than 400 K [19]. Previous analyses have assumed temperatures of 350 K as a rough guide. Once formed, the Ala_7H^+ ions were probed with IR-MPD spectroscopy using the idler output (~10–20 mJ/pulse, tunable from 2000 to 4000 cm^{-1}, with a bandwidth of ~2 cm^{-1}) of a LaserVision KTP/KTA OPO/OPA laser system, tightly focused to a beam diameter ~800 μm, which intersected the ions 400 ns after the UV pulse, in a spatially distinct region downstream from the ionising UV laser beam. IR-MPD spectra were recorded by monitoring the depletion of the parent protonated peptide ion (using active baseline correction [19]) as a function of the IR frequency.

The DFT-based molecular dynamics method and its application to vibrational infrared spectroscopy has been described in many details in our previous papers (Car–Parrinello or Born–Oppenheimer dynamics) [31–33,25,40,41,34,29], including the assignment of the vibrational bands in terms of atomic movements (and our new developed method) [42,40] and the role of temperature in the spectroscopy of gas phase molecules [33,25,41,34,29]. The theoretical set-up follows our previous investigation on the Ala_3H^+ peptide [34]. Briefly, we performed DFT-based Born–Oppenheimer molecular dynamics simulations (BOMD) with the CP2K package [43,44], where the nuclei are treated classically and the electrons quantum mechanically within the DFT (Density Functional Theory) formalism. These simulations solve the Newton's equations of motion of the nuclei at finite temperature, while the electronic wave function is obtained at each nucleus conformation by solving the time-independent Schrödinger equation. Forces that act on the nuclei are derived from the Kohn–Sham energy. We use the Becke, Lee, Yang and Parr (BLYP) gradient-corrected functional [45,46] combined with Goedecker–Teter–Hutter (GTH) pseudopotentials [47–49]. A contracted triple-ζ Gaussian basis set of the type 3s3p2d for (C, N, O) atoms and 3s2p for hydrogen atoms (denoted TZV2P in the CP2K library) is used, where the Gaussian exponents and contraction coefficients have been optimised on molecular calculations as presented in Ref. [50]. A 320 Ryd Plane-wave density cut-off has been applied. The dynamics are performed in the microcanonical NVE ensemble (e.g., constant number of atoms N, volume V, and total energy of the system E) with a time-step of 0.1 fs. The dynamics are divided into an equilibration period (where the atomic velocities can be rescaled) and a production period (purely NVE) of 3–4 ps length where the individual infrared spectra are accumulated. The average temperature of the dynamics is 350 K.

As reviewed in Ref. [29], we have found that finite temperature DFT-based MD with the BLYP functional has been successful

at capturing the main vibrational anharmonicities relevant for the spectroscopy of gas phase alanine peptide chains as well as the vibrational couplings arising from the solvent [32,36]. Other functionals are known in the literature to be better for static frequencies, but our past experience with the BLYP functional in the context of DFT-MD leads us to continue using that functional here. Furthermore, the present investigation is a follow up on our investigation on the Ala_3H^+ peptide, and we want to compare results between these two systems. This can only be done when using the same theoretical set-up.

Calculation of the IR absorption coefficient $\alpha(\omega)$ by means of MD makes use of the relation derived from Linear Response Theory involving the Fourier Transform of the dipole time correlation function [30], as described in our previous works [29]:

$$\alpha(\omega) = \frac{2\pi\beta\omega^2}{3n(\omega)cV} \times \int_{-\infty}^{\infty} dt \langle \mathbf{M}(t) \cdot \mathbf{M}(0) \rangle \exp(i\omega t), \quad (1)$$

where $\beta = 1/kT$, $n(\omega)$ is the refractive index, c is the speed of light in vacuum, V is the volume. $\mathbf{M}$ is the total dipole moment of the system, which is the sum of the ionic and electronic contribution. The IR spectrum of Ala_7H^+ presented in Fig. 2 has been averaged over the seven trajectories performed in the present work. Details on the initial conformations used for these trajectories can be found in the next section. The assignment of the IR active bands into individual atomic displacements has been done using the vibrational density of states (VDOS) formalism [40]. The VDOS is obtained by Fourier transform of the atomic velocity auto-correlation functions:

$$\mathrm{VDOS}(\omega) = \sum_{i=1,N} \int_{-\infty}^{\infty} \langle \mathbf{v}_i(t) \cdot \mathbf{v}_i(0) \rangle \exp(i\omega t) dt \quad (2)$$

where i runs over all atoms of the investigated system. There are no approximations in this formula. The advantage of the VDOS formalism is that all anharmonicities are taken into account in the calculation. The VDOS is furthermore decomposed according to each atom type in order to get a precise interpretation of the vibrational bands in terms of individual atomic motions. This is done by restraining the sum over i in Eq. (2) to the atoms of interest only. We have decomposed the total VDOS into contributions arising from OH, NH, NH^+, C_α H and CH_3 groups, also taking into account whether these groups are Hbonded or not.

3. Conformational dynamics

The initial structures of Ala_7H^+ for the trajectories performed in the present work have been taken from Vaden et al. geometry optimisations [19]. These optimised geometries lie within less than 20 kJ/mol of energy (depending on the level of calculation and whether entropic effects are included) [19]. They are reported in Fig. 1, where one can see globular folded structures in which the N-terminus NH_3^+ is the central element for the folding of the peptide chain to occur. These structures contain charge-solvating $NH^+ \rightarrow O{=}C$ hydrogen bonds involving one ($A_7$1), two ($A_7$2) and three ($A_7$3) NH^+ groups. Briefly, $A_7$3 displays three $NH^+ \cdots O{=}C$ Hbonds with two carbonyls of the chain and the carbonyl of the C-terminus (note the free hydroxyl), $A_7$2 displays two $NH^+ \cdots O{=}C$ Hbonds with one carbonyl of the chain and the carbonyl of the C-terminus (note that the hydroxyl is Hbonded to a chain carbonyl), and $A_7$1 has one $NH^+ \cdots O{=}C$ Hbonds with one chain carbonyl while the carboxylic acid is involved in two Hbonds with another part of the chain. Note that only $A_7$3 has a free COOH hydroxyl. Considering the initial photochemical scheme used for the production of Ala_7H^+ protonated peptides in the IR-MPD spectroscopy experiment [19], it is more than likely that these conformations would be equally produced and possibly contribute to the final IR-MPD spectrum. We thus have performed DFT-based BOMD using all these three initial structures as starting conformations for the dynamics, similarly to our previous investigations on shorter protonated alanine peptides [33,34]. In total, seven trajectories have been calculated, two initiated from $A_7$3 optimised structure, two from $A_7$2, and three from $A_7$1.

At the ~350 K temperature of the dynamics, one observes interesting conformational dynamics directly featured into the hydrogen bonds, either originating from the NH_3^+ or from the COH extremeties of the peptide. Hence, the three Hbonds formed by NH_3^+ in the 0 K $A_7$3 structure are not maintained over the ~3–4 ps trajectory at ~350 K. The conformations sampled in the trajectories originating from that conformation mainly show that two $NH_3^+ \cdots O{=}C$ H-bonds are maintained on average. Three $NH_3^+ \cdots O{=}C$ H-bonds can be formed over short periods of time during the dynamics (typically over a few 100 fs period) before being weakened and broken again. Interestingly, when the three $NH_3^+ \cdots O{=}C$ H-bonds break, one initially looses two of these three H-bonds, before reformation of a second H-bond appears a little bit later in time. Maintaining three $NH_3^+ \cdots O{=}C$ H-bonds at finite temperature is rather difficult, as such a configuration provides a huge constraint over the whole geometry of the peptide. It is thus not surprising to observe that the peptide somehow does not comply easily with such constraint, once temperature and entropic effects are taken into account. Note that the $NH^+ \cdots O{=}C$ Hbond formed with the C-terminus C=O of the chain does not appear more (or less) robust than any $NH^+ \cdots O{=}C$ Hbond formed with the chain carbonyl groups, and this Hbond breaks and (re)forms as much as the other ones in time. Note also that the C-terminus OH group remains free of any hydrogen bonding over the trajectories initiated from the $A_7$3 optimised structure. The main structural parameters of the peptide chain are maintained close to the values of the optimised geometry, although fluctuations in the dihedral angles are observed over time, as expected from the temperature of the system.

Dynamics initiated from the $A_7$2 optimised structure show that the two H-bonds formed between NH_3^+ and its surrounding are maintained on average over the finite temperature dynamics, while the fate of the $(CO)OH \cdots O{=}C$ H-bond is more uncertain. This H-bond is indeed maintained on average over one trajectory while it breaks ~1 ps after the beginning of the other trajectory. Interestingly, the $OH \cdots O$ Hbond-length goes up to 3.0 Å, the OH still facing the oxygen atom of the carbonyl, and thermal fluctuations allow the OH and carbonyl groups to reform their H-bond after ~1 ps. These two trajectories show that the free energy barrier to break and form such a $OH \cdots O{=}C$ H-bond in the peptide is low and easily overcome in room temperature trajectories. Looking at the general organisation of the peptide skeleton, there is probably no easy pathway opened, at the average internal energy of the system, to go from conformations without a $OH \cdots O{=}C$ H-bond to an energetically more favorable (at least as energetically favorable) situation. That would certainly require high energy barriers to be overcome corresponding to major structural rearrangements of the chain to be generated, out of reach of the present temperature dynamics and short time-scale dynamics.

The dynamics originating from $A_7$1 structure are highly instructive. The optimised structure displays one strong H-bond between NH_3^+ and one carbonyl of the peptide chain, while a highly distorted (140° angle) and longer Hbond-length (1.80 Å) can nonetheless be seen between a second NH^+ and another carbonyl of the chain. One immediate consequence of the finite temperature dynamics is the extremely fast loss of the $OH \cdots O{=}C$ H-bond from the 0 K optimised structure. This leads to a reorganisation of the local structure of the peptide chain. For instance, in one trajectory, one observes that at one-third of the trajectory, the distance between the OH and the carbonyl group has reached 6 Å. Simultaneously, the distance

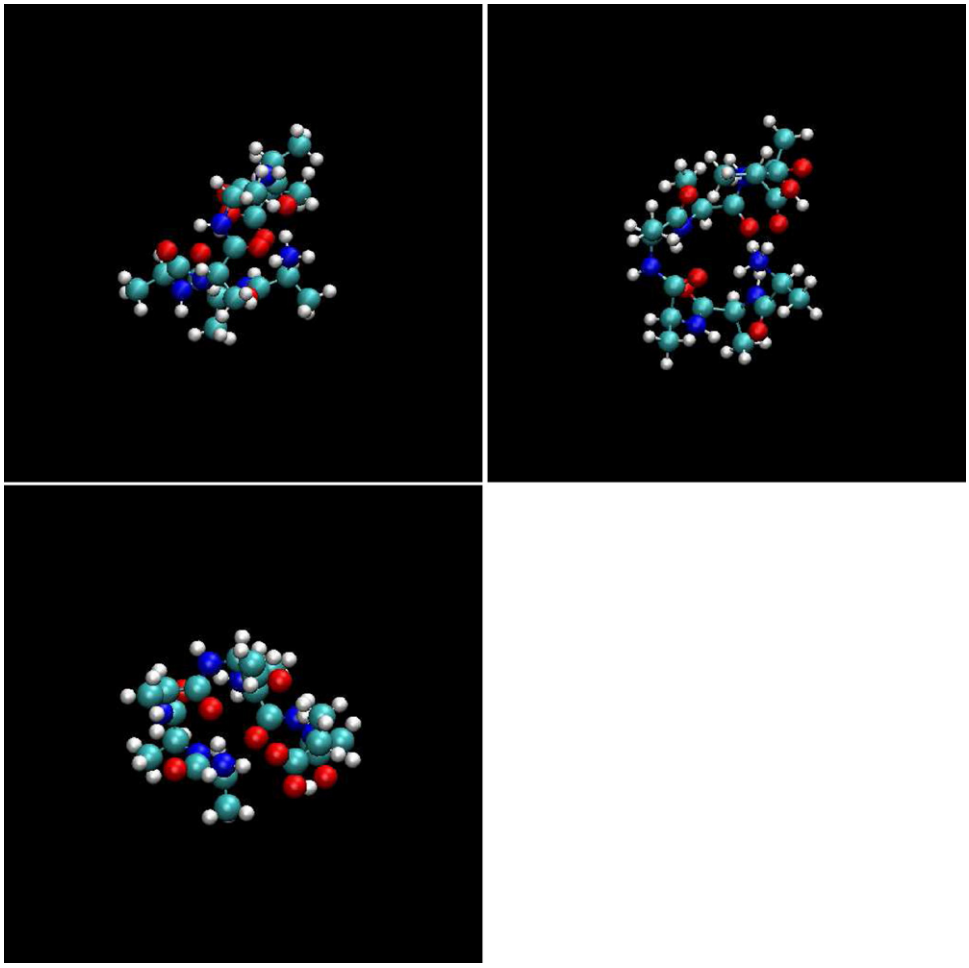

Fig. 1. Optimised globular folded structures of Ala_7H^+ protonated peptide extracted from Ref. [19] and used as starting conformations for the DFT-based BOMD dynamics performed in the present work. Order of the structures (top left to right, and to bottom): $A_7$1, $A_7$2, $A_7$3, respectively displaying one, two and three N–$H^+\cdots$O=C hydrogen bonds in the optimised structures.

between that very same carbonyl and the initially free NH^+ of the NH_3^+ group decreases from 3 Å to 1.70 Å on average, and remains at that average distance for the rest of the dynamics. There is thus an exchange of Hbond formed by this carbonyl with the surrounding Hbond donors of the peptide chain. The same behaviours are observed in all trajectories initiated from $A_7$1, with different timescales. Depending on the thermal fluctuations obtained within the same trajectory or between the different trajectories performed, one can observe a very nice conformational dynamics of the peptide arising around the NH_3^+ group, with alternate situations where one, two and even three $NH_3^+\cdots$ O=C H-bonds are formed in time. The OH group and C=O group of the C-terminus are on average not involved in H-bonding at finite temperature.

As a summary, out of the seven BOMD trajectories performed in the present work on Ala_7H^+ protonated peptide, two provide one $NH^+\cdots$O=C H-bond formed on average, as the statistically most relevant event for the $NH^+\cdots$O=C H-bond situation, five provide two such Hbonds on average (note that portions of other trajectories also display that situation in transitory periods of time), and one trajectory can be used for the three $NH^+\cdots$O=C Hbond situation over a sufficient period of time for the Fourier transformation necessary for the calculation of the IR spectrum (Eq. (1)). The two $NH^+\cdots$O=C H-bond situation is thus statistically the most observed (most probable) at finite temperature. At 350 K, we have found that these Hbonds can form and break easily, and the more Hbonds that can be simultaneously formed the weaker and thus the easier they can break. Furthermore, the (CO)OH C-terminus hydroxyl of the Ala_7H^+ peptide is on average not hydrogen bonded to its surrounding, although situations where it can form Hbonds have been observed in a few trajectories, but with a less statistical occurrence. Over the rather limited periods of time of the dynamics (4 ps), only the dynamical behaviour of forming and breaking of Hbonds has been observed, no other remarkable structural reorganisation of the chain could be seen (as this would require much longer simulations).

4. Infrared spectroscopy and vibrational assignments

The average IR spectrum extracted from the seven BOMD trajectories performed in the present work is presented in Fig. 2. We have considered a simple average, based on the idea that all three initial conformers are likely to be formed in the experiment (considering the way the peptides are produced) and thus equally contribute to the final IR-MPD spectrum without any consideration of relative energy (or Boltzmann weight). This follows the same strategy as the one used in our previous work on Ala_3H^+ [34]. The VDOS (vibrational density of states) signatures primarily used here for the assignment of the IR active bands are reported in Fig. 3, and their interpretations follow the general outlines explained in Ref. [40].

The IR active band found at 3560 cm^{-1} in our calculations is solely due to the vibrational signature of free (C)O–H stretching (see

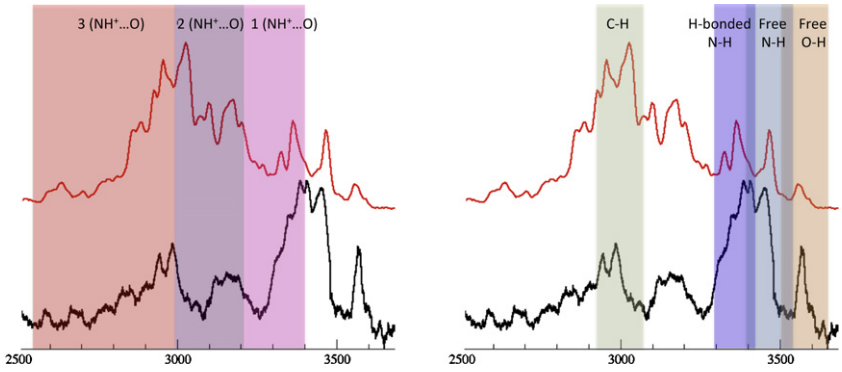

Fig. 2. Experimental IR-MPD spectrum from Ref. [19] (bottom, black line) and dynamical spectrum (top, red line) obtained as an average over the seven trajectories of Ala_7H^+ protonated peptide performed in the present work. The spectra have been color coded. Left: N–H^+ stretchings according to the number of hydrogen bonds they form (3 Hbonds-red, 2 Hbonds-violet, 1 Hbond-pink); right: C–H (green), N–H (blue and light-blue) and O–H (orange) stretchings. See text for the assignments.

Fig. 3). As already emphasized in the previous section, a free O–H is encountered in the majority of conformations explored along the dynamics of Ala_7H^+ at room temperature, thus the band that is observed in the calculations and in the experiment showing up at 3560 cm^{-1}. As we have seen, there are nonetheless situations where the C-terminus O–H group is hydrogen bonded to a carbonyl group of the peptide chain, and this gives rise to red-shifted stretching signatures of this group, as illustrated in Fig. 3. Furthermore, the O–H···O=C H-bonds formed are very dynamical and vibrationally anharmonic, which gives rise to the large vibrational domain (2600–3600 cm^{-1}) where signatures of Hbonded O–H are recorded (see Fig. 3). Note here, as we have emphasized in the structural analyses in the previous section, that situations where O–H is involved in H-bonding and situations where it is not involved coexist within the same trajectory, so that it is not surprising to recover the 3560 cm^{-1} signature in the VDOS distribution of Hbonded O–H (both situations have not been separated for the analyses). The vibrational signatures of H-bonded O–H being spread over the 2600–3600 cm^{-1} domain, they will definitely be participating to any IR active band within that domain. Thus the IR active bands seen at 3300–3500 cm^{-1}, 3150–3250 cm^{-1} and around 3000 cm^{-1} will contain such participation from H-bonded O–H stretchings. Judging by the signatures in the 2600–2900 cm^{-1} domain in the experiment, one can anticipate that these movements contribute to the low amplitude IR bands seen in the experimental spectrum and in our simulations in that frequency region.

The N–H stretching signatures of the amide groups of the peptide chain are recorded in the 3300–3520 cm^{-1} domain, with non hydrogen bonded N–H groups displaying signatures roughly in the 3400–3520 cm^{-1} range (Fig. 3), and H-bonded N–H groups displaying signatures roughly in the 3300–3440 cm^{-1} (Fig. 3). These two bands slightly overlap as the N–H movements are highly dynamical: the H-bonds formed between N–H and their carbonyl partners undergo a certain dynamics with forming and breaking situations of the N–H···O=C H-bond in time. The amide N–H signatures do not depend on the subtle differences observed in the

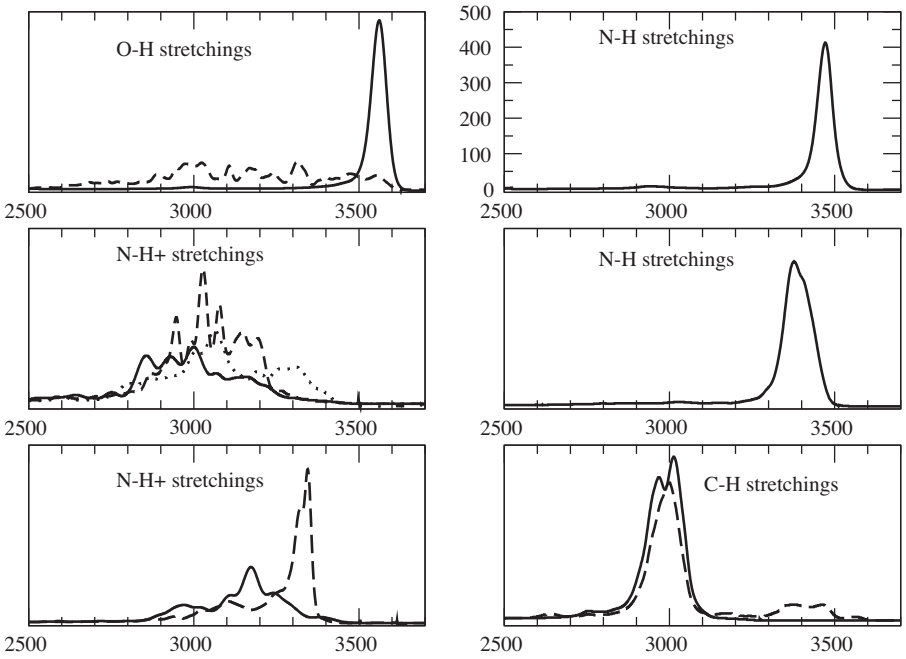

Fig. 3. VDOS decompositions used in the present analyses of the dynamical spectrum for the assignment of the vibrational bands. Top left: O–H (free O–H in solid line, Hbonded O–H in dashed line); middle left: Hbonded N–H^+ (solid line: one Hbond on average; dashed line: two Hbonds on average; dotted line: three Hbonds on average); bottom left: non Hbonded N–H^+ (solid line: case extracted from the "one Hbond on average" situations; dashed line: case extracted from the "two Hbonds on average" situations); top right: free N–H; middle right: H-bonded N–H; bottom right: H atoms from the C_α–H groups (dashed line) and from the CH_3 groups (solid line).

peptide skeleton induced by the number of inter-molecular hydrogen bonds that the N-terminus NH_3^+ group can form (and discussed below).

C–H signatures arising from the C_α groups and methyl Alanine residues are commonly placed in the 2920–3050 cm^{-1} region. One also observes C_α–H signatures within the 3330–3480 cm^{-1} domain, overlapping with the N–H stretchings.

Vibrational signatures of N–H^+ from the NH_3^+ N-terminus of the peptide clearly reflect strong vibrational anharmonicities of the N–H^+ stretching and dynamical behaviours of the N–$H^+\cdots$O=C H-bonds, both resulting in VDOS bands shifted to low frequencies (mostly below 3200 cm^{-1}) and spread over the 2600–3400 cm^{-1} frequency domain (Fig. 3). Depending on the number of H-bonds the NH_3^+ group is involved in (i.e., one, two or three, see previous section for details), one can see that the N–H^+ signatures are located in different frequency domains. We need to recall here that distinguishing the situations where one, two or three Hbonds are formed between NH_3^+ and surrounding Hbond acceptors along the trajectories is not trivial, as these Hbonds are highly dynamical. Along one single trajectory, several situations can therefore be encountered, i.e., one and two Hbonds formed for instance at different times along the trajectory, and both signatures will be recorded within the corresponding VDOS over that trajectory, which obviously complicates a precise assignment of the vibrational features of NH_3^+ in the peptide. The trajectories have been labeled as a "one" or "two" "Hbonds case" on average, but the other situations will still be included within the VDOS signatures. Note that the relative weight of both situations is naturally taken into account in the time correlation function calculation. We have taken into account the whole length of the trajectories for the calculation of the IR and VDOS spectra, i.e., we have not separated the trajectories into smaller time-length pieces where only one kind of N–$H^+\cdots$O=C H-bonds exist. As these H-bonds are very dynamical in essence in all trajectories (whatever the number of N–$H^+\cdots$O=C hydrogen bonds formed on average), reducing the trajectories to smaller portions of times where exactly one N–$H^+\cdots$O=C H-bond (respectively, two or three N–$H^+\cdots$O=C H-bonds) are formed would involve too short periods of time for the correlation function and its Fourier Transform to be properly defined. As a result, the more the trajectory is composite in terms of number of H-bonds formed by the NH_3^+ N-terminus group in time (one, two and three H-bonds possibly alternating within the same trajectory) the more diverse the signatures of the N–H^+ stretch. The nomenclature used here refers to the most probable number of N–$H^+\cdots$O=C H-bonds formed on average, but nonetheless also include a few other situations encountered along the trajectories related to that average state. This is clear in all cases depicted in Fig. 3, also more generally illustrating the complexity of assigning vibrational bands for dynamical systems.

We find that when NH_3^+ is involved in one H-bond only on average, the N–H^+ stretching is mostly comprised between 2600 and 3050 cm^{-1} (solid line in Fig. 3), with a featureless tail of lower amplitude roughly extending up to 3200 cm^{-1}. When NH_3^+ forms two intermolecular H-bonds on average, ν(N–H^+) appears in the 2900–3200 cm^{-1} domain (dashed line in Fig. 3). The signatures ascribed to the situations where NH_3^+ is involved in three H-bonds deserve more attention. The VDOS presented in Fig. 3 (dotted line) clearly shows two separate bands, one in the 2970–3100 cm^{-1} range and one in the 3200–3400 cm^{-1} domain. The trajectory recorded as giving rise to an "average three Hbonds" situation of NH_3^+, also contains a "two Hbonds" situation over a substantial amount of time along the trajectory. This thus gives rise to the two frequency domains in the vibrational spectrum, where the 2970–3100 cm^{-1} part is certainly mostly due to the situations where NH_3^+ forms two Hbonds on average while the 3200–3400 cm^{-1} part certainly arises from the situations where NH_3^+ forms three Hbonds on average.

The more red-shifted ν(N–H^+) stretching bands (i.e., lower frequency ν(N–H^+)) are thus obtained for Ala_7H^+ conformations where one N–$H^+\cdots$O=C H-bond is formed on average, i.e., 2600–3050 cm^{-1}. These low frequencies correspond to a highly anharmonic N–$H^+\cdots$O=C H-bond, in comparison to N–H$\cdots$O=C H-bonds, for which the spectral signature is centered around 3380 cm^{-1}. The anharmonicities sampled as well as the dynamical behaviour of this H-bond can be seen in the ripples of low amplitudes between 2600 and 2800 cm^{-1} in the VDOS curve, and in the several VDOS peaks appearing in the 2800–3050 cm^{-1} frequency range. The VDOS tail above 3100 cm^{-1} is most probably due to the situations where two N–$H^+\cdots$O=C H-bonds also appear on short time-scales along the trajectories, hence the spectral overlap between the "two Hbonds cases" and "one Hbond cases" in the 3100–3200 cm^{-1} domain. Similarly, the ν(N–H^+) stretching signatures obtained from the trajectories where two N–$H^+\cdots$O=C H-bonds are formed on average, also include signatures arising from the smaller periods of time when one N–$H^+\cdots$O=C H-bond situations are encountered, thus the spectral overlap in the 2900–3000 cm^{-1} domain (between solid and dashed lines). Hence, we believe that the 3000–3200 cm^{-1} vibrational domain is the signature of two N–$H^+\cdots$O=C H-bonds formed on average, while the 2600–3000 cm^{-1} domain arises from one N–$H^+\cdots$O=C H-bond conformations. Finally, the three N–$H^+\cdots$O=C H-bonds average situation is seen in trajectories where both three and two H-bonds alternate along the trajectories (the "three H-bonds" situation being slightly predominant over the "two H-bonds" situation). As a result, the 3000–3100 cm^{-1} VDOS band mostly arises from the "two H-bonds" situation (compatible with the previous analysis above) while the 3200–3400 cm^{-1} VDOS band arises from ν(N–H^+) signature of "pure three H-bonds" conformations.

One therefore concludes that there is a loss of vibrational anharmonicity of the ν(N–H^+) stretching motion when going from "one N–$H^+\cdots$O=C H-bond" Ala_7H^+ conformations, to "two H-bonds" and "three N–$H^+\cdots$O=C H-bonds" Ala_7H^+ conformations. The more anharmonic conformations provide ν(N–H^+) stretching signatures in the 2600–3000 cm^{-1} frequency domain, the intermediate anharmonic ν(N–H^+) stretching signatures are in the 3000–3200 cm^{-1} range, and the less anharmonic ν(N–H^+) stretching signatures are in the 3200–3400 cm^{-1} range. These latter ν(N–H^+) are overlapping with the Hbonded amide ν(N–H) stretchings.

Fig. 2 presents the comparison between the IR-MPD experimental data extracted from Ref. [19] and the present final IR spectrum extracted from the seven trajectories on Ala_7H^+ peptide. Bands have been colored (same color coding in both the experiment and simulation) according to the nature of the stretching assignments. It is clear that all experimental spectral features are obtained in the dynamical spectrum. As always when comparing IR-MPD and calculated spectra (harmonic spectra from static optimisations or dynamical spectra as here), one must be extremely cautious about discussing IR intensities, as they are not comparable between experiments and simulations [29]. Experimental intensities correspond to a fragmentation ratio in IR-MPD while the calculated intensities correspond to a one-photon absorption cross section. Such caution does not apply to band positions and band shapes, which can then be safely compared. Saying that, it is not surprising to observe that spectral intensities do not generally match between experiment and simulation. On the other hand, the band shapes and positions agree extremely well between both, as we shall discuss into more details now. We recall here that no scaling or global translation of the bands has been done in the present calculation. The excellent agreement in the calculated band positions results from the dynamics using the BLYP functional. Overall, the dynamical signatures match very well with the IR-MPD features in terms of band-positions and band-widths. In particular, the experimental feature at 3100–3230 cm^{-1} can immediately be seen in the

dynamical spectrum calculated here for Ala_7H^+ protonated peptide, where no such band could be observed for the shorter Ala_3H^+ peptide [34].

The band located around 3560 cm^{-1} in the experiment and simulation and corresponding to the free O–H stretching, match nicely, including the shoulder at ~3590 cm^{-1}. The broad band roughly extending between 3300 and 3480 cm^{-1} related to the N–H stretchings match nicely between experiment and simulation. The experimental band is clearly composed of at least two sub-bands, one between 3300 and 3400 cm^{-1}, the other between 3400 and 3480 cm^{-1}. The calculated spectrum shows two such sub-domains, with a more definite separation between these bands at 3400 cm^{-1}. From the VDOS analysis presented above, we have seen that these two spectral sub-domains are respectively due to non Hbonded N–H (higher frequency part) and to Hbonded N–H (lower frequency part). As previously observed for Ala_3H^+ [34], the broadness of this latter 3300–3400 cm^{-1} band as well as the supplementary substructures that can be seen within that band, arise from the H-bond dynamics, where alternate sequences of breaking and reforming occur at finite temperature. The supplementary experimental substructures in the 3300–3400 cm^{-1} band are composed of four peaks, respectively located at ~3410, 3388, 3355 and 3320 cm^{-1}, that can also be seen in the dynamical simulated spectrum. The simulation nonetheless provides more separate peaks than the experiment does, but that should easily be explained by the rather small number of trajectories used for the final dynamical spectrum. More statistics would likely lead to a better resolution of the simulated spectral bands, and thus to an even better agreement with the experiment in that frequency domain. This was already observed in our previous work on Ala_3H^+ [34]. Despite that remark, the agreement in the 3300–3500 cm^{-1} domain is remarkable, and clearly out of reach of static harmonic calculations [19]. N–H^+ stretching signatures also show up within the tail of the 3300–3400 cm^{-1} band, arising from Ala_7H^+ conformations where the NH_3^+ group can be involved in three Hbonds on average. This contributes to the broadening and "shoulder" of the 3300–3500 cm^{-1} band around 3300 cm^{-1}. Note also that the shoulder located at 3510 cm^{-1} in the experiment is nicely present in our calculation. The supplementary band observed in the 3030–3300 cm^{-1} spectral domain of Ala_7H^+ which was absent for the shorter peptides (see Ref. [34] for our previous comparison between dynamical spectrum and experiment in the case of Ala_3H^+) is remarkably reproduced by the present dynamical spectrum. The band extending between 3100 and 3240 cm^{-1} in the experiment is present in the dynamical spectrum, its width being slightly smaller (the band extends between 3125 and 3230 cm^{-1} in the calculation). The experimental shoulder seen at 3250 cm^{-1} is also present in the calculation, slightly blue-shifted by 15 cm^{-1}. This band is entirely due to N–H^+ stretches arising from Ala_7H^+ conformations where the NH_3^+ N-terminus is involved in two hydrogen bonds on average. Note that Hbonded O–H stretches obviously also contribute to this spectral domain, as can be seen from the related VDOS signatures. Although we have found that Ala_7H^+ peptide conformations displaying such Hbonded O–H are not the most statistically representative, they do exist, and these highly delocalized and anharmonic vibrational movements will definitely contribute to the intensity of the observed 3030–3300 cm^{-1} band. Remarkably, the two peaks seen at 3035 and 3065 cm^{-1} in the experiment are also present in the simulation, with higher intensities and slightly blue-shifted from the experiment (roughly +40 cm^{-1}). These peaks are also due to N–H^+ and Hbonded O–H stretches, where singly and doubly Hbonded NH_3^+ conformations will likely contribute. The 2500–3000 cm^{-1} experimental part of the spectrum is also remarkably reproduced by the dynamical spectrum. C–H stretchings from CH_3 and $C_\alpha H$ groups contribute to the experimental 2920–3000 double bands, as was already observed for the Ala_3H^+ peptide [34]. Clearly, the C–H stretches show up in the two peaks, at 2945 and 2985 cm^{-1} in the experiment and respectively at 2955 and 3025 cm^{-1} in the calculation, and their shapes match well between experiment and simulation. But this region is clearly more complex, as we have shown that highly anharmonic vibrations of the singly Hbonded NH_3^+ conformations and Hbonded hydroxyl groups have multiple vibrational signatures in that domain. The bands observed in the experiment between 2500 and 2900 cm^{-1} all arise from conformations where either the hydroxyl of the C-terminus is involved in Hbonds and/or the N-terminus is involved in one Hbond only. Note also that N–H^+ and O–H contribute to the 2960–3030 cm^{-1} bands, increasing the C–H intensities also present in that spectral domain.

5. Conclusions and perspectives

The present investigation reports DFT-based Born–Oppenheimer molecular dynamics simulations of the gas phase Ala_7H^+ protonated peptide, in order to unravel the structure and dynamics of the peptide and its Infrared vibrational signatures. We have found that, at 350 K temperature, the most statistically relevant conformations adopted by the globular folded Ala_7H^+ peptide have the NH_3^+ N-terminus involved in two $NH^+ \rightarrow O{=}C$ charge-solvated hydrogen bonds. This type of conformations give rise to the 3100–3250 cm^{-1} active band observed in the IR-MPD of the Ala_7H^+ peptide and is absent for smaller peptide chain lengths. Note that the dynamics of these conformations also reveal that the hydroxyl O–H group at the C-terminus of the peptide can be either Hbonded to its C=O surroundings as well as not, with highly dynamical behaviours of the O–H···O=C Hbond (with alternate breaking and forming of the Hbond along the time). Such situations give rise to the 3560 cm^{-1} IR active band in the IR-MPD spectrum of Ala_7H^+ (free O–H), as well as participations to the small amplitude IR-MPD bands that can be observed in the 2500–2900 cm^{-1} domain (Hbonded anharmonic O–H). Conformations of Ala_7H^+ with one $NH^+\cdots O{=}C$ on average can also occur, with highly dynamical and anharmonic $NH^+\cdots O{=}C$ Hbonds. This results in the 2500–3000 cm^{-1} vibrational signatures, very similar to the case of the Ala_3H^+ peptide that we have previously investigated [34]. In particular, the small amplitude peaks seen between 2500 and 2900 cm^{-1} come from anharmonic behaviours of the strong $NH^+\cdots O{=}C$ Hbond formed (already seen in Ala_3H^+ [34]). These "one Hbond case" conformations also provide an enhancement of the C–H stretching activities between 2900 and 3000 cm^{-1}. Finally, conformations with a fully charge-solvated NH_3^+ N-terminus group (three $NH^+\cdots O{=}C$ Hbonds formed on average) are rare, but can occur nonetheless, as shown from the dynamics performed here. In that case, the N–H^+ stretch signature has lost most of the anharmonicities seen for the two Hbonds and one Hbond situations, and its signatures can be found at the foot (~3300 cm^{-1}) of the N–H Hbonded amide stretchings, thus giving rise to the shoulder of the IR-MPD 3300–3500 cm^{-1} band.

The dynamics performed here nicely provide a clear understanding of the IR-MPD features experimentally recorded, with an excellent matching of the dynamically simulated IR spectrum with the experiment in terms of band-positions and band-shapes. In particular, the diverse vibrational anharmonicities displayed by the N–H^+ stretches depending on the number of simultaneous hydrogen bonds that the NH_3^+ can form at the N-terminus of the Ala_7H^+ peptide chain, are remarkably reproduced by the dynamics at finite temperature. This gives rise to a proper understanding of the different IR active bands, especially the supplementary band between 3100 and 3300 cm^{-1} present for the Ala_7H^+ peptide and absent for the smaller peptide chain lengths. Such agreement between experiment and calculation for the vibrational signatures is out of reach of static harmonic calculations. Temperature has to be taken into

account in order to get a proper view of the conformational dynamics of the peptide, and here in particular we have shown that the two $N–H^+\cdots O{=}C$ Hbonds situations are the most probable, once temperature and entropic effects are taken into account. Vibrational anharmonicities are naturally taken into account in the dynamical treatment of the movements, and this has once more been illustrated in the present work. In particular, the different behaviours of stretchings of $N–H^+$ when one, two and three Hbonds are simultaneously formed, have been revealed in the present work, giving rise to three separate vibrational domains for the $N–H^+$ stretch motion. Our results on the $N–H^+$ stretching motions in relation with the number of hydrogen bonds formed by the NH_3^+ group, can be used as general guidelines in order to precisely interpret IR-MPD spectra of molecules containing NH_3^+ groups, taking into account vibrational anharmonicities.

Acknowledgments

This work was granted access to the HPC resources of IDRIS under the allocations 2008–2010[72484] made by GENCI (Grand Equipement National de Calcul Intensif) in France. MPG acknowledges support from Genopole-France through the program 'ATIGE' Action Thématique Incitative de Génopole. LCS is grateful to the Royal Society for a University Research Fellowship, to The Leverhulme Trust (Grant F/08788G), and to Corpus Christi College, Oxford for support. MPG and LCS are grateful to the PHC-Alliance Program for collaborative financial support.

References

[1] J.P. Schermann, Spectroscopy and Modeling of Biomolecular Building Blocks, Elsevier Science, Amsterdam, The Netherlands, 2007.
[2] T.R. Rizzo, J.A. Stearns, O.V. Boyarkin, Int. Rev. Phys. Chem. 28 (2009) 481.
[3] J.P. Simons, Mol. Phys. 107 (2009) 2435.
[4] J.A. Stearns, O.V. Boyarkin, T.R. Rizzo, J. Am. Chem. Soc. 129 (2007) 13820.
[5] J.A. Stearns, S. Mercier, C. Seaiby, M. Guidi, O.V. Boyarkin, T.R. Rizzo, J. Am. Chem. Soc. 129 (2007) 11814.
[6] V. Brenner, F. Piuzzi, I. Dimicoli, B. Tardivel, M. Mons, J. Phys. Chem. A 111 (2007) 7347.
[7] A.M. Rijs, B.O. Crews, M.S. de Vries, J.S. Hannam, D.A. Leigh, M. Fanti, F. Zerbetto, W.J. Buma, Angew. Chem.-Int. Ed. 47 (2008) 3174.
[8] P.D. Carnegie, B. Bandyopadhyay, M.A. Duncan, J. Phys. Chem. A 112 (2008) 6237.
[9] G.E. Douberly, A.M. Ricks, B.W. Ticknor, W.C. Mckee, P.V.R. Schleyer, M.A. Duncan, J. Phys. Chem. A 112 (2008) 1897.
[10] M. Kolaski, H.M. Lee, Y.C. Choi, K.S. Kim, P. Tarakeshwar, D.J. Miller, J.M. Lisy, J. Chem. Phys. 126 (2007) 074302.
[11] Z.M. Loh, R.L. Wilson, D.A. Wild, E.J. Bieske, J.M. Lisy, N.B. Njegic, M.S. Gordon, J. Phys. Chem. A 110 (2006) 13736.
[12] J. Lemaire, P. Boissel, M. Heninger, G. Mauclaire, G. Bellec, H. Mestdagh, A. Simon, S.L. Caer, J. Ortega, F. Glotin, P. Maitre, Phys. Rev. Lett. 89 (2002) 273002–273011, and references therein.
[13] J. Oomens, G. Meijer, G.V. Helden, J. Phys. Chem. A 105 (2001) 8302.
[14] C. Kapota, J. Lemaire, P. Maitre, G. Ohanessian, J. Am. Chem. Soc. 126 (2004) 1836.
[15] C.F. Correia, P.O. Balaj, D. Scuderi, P. Maitre, G. Ohanessian, J. Am. Chem. Soc. 130 (2008) 3359.
[16] T.D. Vaden, T.S.J.A. de Boer, J.P. Simons, L.C. Snoek, Phys. Chem. Chem. Phys. 10 (2008) 1443.
[17] M.F. Bush, J. Oomens, R.J. Saykally, E.R. Williams, J. Am. Chem. Soc. 130 (2008) 6463.
[18] N.A. Macleod, J.P. Simons, Mol. Phys. 104 (2006) 3317.
[19] T.D. Vaden, T.S.J.A. de Boer, J.P. Simons, L.C. Snoek, S. Suhai, B. Paizs, J. Phys. Chem. A 112 (2008) 4608.
[20] C. Kapota, G. Ohanessian, Phys. Chem. Chem. Phys. 7 (2005) 3744.
[21] B. Lucas, G. Gregoire, J. Lemaire, P. Maitre, J.M. Ortega, A. Rupenyan, B. Reimann, J.P. Schermann, C. Desfrancois, Phys. Chem. Chem. Phys. 6 (2004) 2659.
[22] B. Lucas, G. Gregoire, J. Lemaire, P. Maitre, F. Glotin, J.P. Schermann, C. Desfrancois, Int. J. Mass Spectrom. 243 (2005) 105.
[23] W. Chin, F. Piuzzi, J.P. Dognon, I.L. Dimicoli, B. Tardivel, M. Mons, J. Am. Chem. Soc. 127 (2005) 11900.
[24] J.Y. Salpin, S. Guillaumont, J. Tortajada, L. MacAleese, J. Lemaire, P. Maitre, Chem. Phys. Chem. 8 (2007) 2235.
[25] G. Grégoire, M.P. Gaigeot, D.C. Marinica, J. Lemaire, J.P. Schermann, C. Desfrançois, Phys. Chem. Chem. Phys. 9 (2007) 3082.
[26] K. Pagel, P. Kupser, F. Bierau, N.C. Polfer, J.D. Steill, J. Oomens, G. Meijer, B. Koksch, G. von Helden, Int. J. Mass Spectrom. 283 (2009) 161.
[27] N.C. Polfer, J. Oomens, Mass Spectrom. Rev. 28 (2009) 468.
[28] V. Gabelica, F. Rosu, E. de Pauw, J. Lemaire, J.C. Gillet, J.C. Poully, F. Lecomte, G. Gregoire, J.P. Schermann, C. Desfrancois, J. Am. Chem. Soc. 130 (2008) 1810.
[29] M.P. Gaigeot, Phys. Chem. Chem. Phys. 12 (2010) 3336.
[30] D. McQuarrie, Statistical Mechanics, Harper-Collins Publishers, New York, 1976.
[31] M.P. Gaigeot, M. Sprik, J. Phys. Chem. B 107 (2003) 10344.
[32] M.P. Gaigeot, R. Vuilleumier, M. Sprik, D. Borgis, J. Chem. Theor. Comput. 1 (2005) 772.
[33] C. Marinica, G. Grgoire, C. Desfranois, J.P. Schermann, D. Borgis, M.P. Gaigeot, J. Phys. Chem. A 110 (2006) 8802.
[34] A. Cimas, T.D. Vaden, T.S.J.A. de Boer, L.C. Snoek, M.P. Gaigeot, J. Chem. Theor. Comput. 5 (2009) 1068.
[35] A. Cimas, P. Maitre, G. Ohanessian, M.P. Gaigeot, J. Chem. Theor. Comput. 5 (2009) 2388.
[36] M.P. Gaigeot, Phys. Chem. Chem. Phys. 12 (2000) 10198.
[37] N.-T.V. Oanh, C. Falvo, F. Calvo, M. Basire, M.-P. Gaigeot, P. Parneix, Phys. Chem. Chem. Phys., submitted for publication.
[38] N. MacLeod, J. Simons, Mol. Phys. 105 (2007) 689.
[39] T.D. Vaden, T.S.J.A. de Boer, N.A. MacLeod, E.M. Marzluff, J.P. Simons, L.C. Snoek, Phys. Chem. Chem. Phys. 9 (2007) 2549.
[40] M.P. Gaigeot, M. Martinez, R. Vuilleumier, Mol. Phys. 105 (2007) 2857.
[41] M.P. Gaigeot, J. Phys. Chem. A 112 (2008) 13507.
[42] M. Martinez, M.P. Gaigeot, D. Borgis, R. Vuilleumier, J. Chem. Phys. 125 (2006) 144106.
[43] J. VandeVondele, M. Krack, F. Mohamed, M. Parrinello, T. Chassaing, J. Hutter, Comput. Phys. Commun. 167 (2005) 103.
[44] The cp2k developers group, 2004. http://cp2k.berlios.de/.
[45] A. Becke, Phys. Rev. A 38 (1988) 3098.
[46] C. Lee, W. Yang, R. Parr, Phys. Rev. B 37 (1988) 785.
[47] M. Krack, Theor. Chem. Acc. 114 (2005) 145.
[48] S. Goedecker, M. Teter, J. Hutter, Phys. Rev. B 54 (1996) 1703.
[49] C. Hartwigsen, S. Goedecker, J. Hutter, Phys. Rev. B 58 (1998) 3641.
[50] J. VandeVondele, J. Hutter, J. Chem. Phys. 127 (2007) 114105.